SKB TECHNICAL REPORT 87-18

Calculation of gas migration in fractured rock

Roger Thunvik
Royal Institute of Technology
Stockholm, Sweden

Carol Braester
Israel Institute of Technology
Haifa, Israel

Stockholm, September 1987

SVENSK KÄRNBRÄNSLEHANTERING AB
SWEDISH NUCLEAR FUEL AND WASTE MANAGEMENT CO
BOX 5864 S-102 48 STOCKHOLM
TEL 08-665 28 00 TELEX 13108-SKB

CALCULATION OF GAS MIGRATION IN FRACTURED ROCK

Roger Thunvik
Royal Institute of Technology
Stockholm, Sweden

Carol Braester
Israel Institute of Technology
Haifa, Israel

Stockholm, September 1987

CALCULATION OF GAS MIGRATION IN FRACTURED ROCK

Roger Thunvik
Royal Institute of Technology
Stockholm, Sweden

Carol Braester
Israel Institute of Technology
Haifa, Israel

Stockholm, September 1987

ABSTRACT

Medium and low level radioactive waste repository caverns are planned to be located in fractured hard rock formations at a depth of about 50 metres below the sea level. Chemical reactions in the stored waste will result in gas (hydrogen) production in a saturated water environment. Under such conditions the gas will displace the water from the fractures and migrate towards the surface and finally be released through the sea bottom. The lateral gas movement is considered negligible and the computations were performed under the assumption of vertical flow. Calculations are presented for rock properties characteristic to the Forsmark area. The rock permeability was determined by flow tests in vertical boreholes. It is assumed that the permeability distribution obtained from these boreholes is representative also for the permeability distribution along the repository cavern. Calculations were worked out for two different types of boundary conditions, one in which a constant gas flow rate equivalent to a gas production of 33000 kg/year was assumed and the other in which a constant gas cushion of 0.5 metres was assumed. For the permeability distribution considered, the breakthrough at the sea bottom occurred within one hour. The gas-water displacement took place mainly through the fractures of high permeability and practically no flow took place in the fractures of low permeability. A gas cushion was formed during a very short period. The gas breakthrough at the sea bottom results in a sudden drop in pressure and backflow in the low permeability classes of fractures.

CONTENTS

LIST OF FIGURES

NOMENCLATURE

symbol	description	dimension
B	cavern width	L
b	fracture width	L
c^f	compressibility of the fluid	$M^{-1}Lt^2$
c^r	compressibility of the rock matrix	$M^{-1}Lt^2$
g	acceleration of gravity	Lt^{-2}
k	permeability	L^2
l	fracture spacing	L
M	molecular weight of the gas	M $mole^{-1}$
n_i	fracture frequency of fracture category i	-
p	pressure	$ML^{-1}t^{-2}$
p_c	capillary pressure	$ML^{-1}t^{-2}$
q^n	normal flux	Lt^{-1}
Q	mass rate of gas production	$ML^{-3}t^{-1}$
R	gas constant	$ML^2t^{-2}T^{-1}mole^{-1}$
t	time	t
S_{gr}	residual gas saturation	-
S_{wir}	irreducible water saturation	-
T	temperature	T
u	volumetric rate of flow per unit area	Lt^{-1}
v	velocity	Lt^{-1}
Z	correction factor for real gases	-

greek	description	dimension
ρ	density	ML^{-3}
μ	dynamic viscosity	$ML^{-1}t^{-1}$
ϕ	porosity	-
Ψ	basis function	-

subscripts

i	fracture category

superscripts

w	water
g	gas
(i)	iteration level
I, J, K	node number

1. INTRODUCTION

In Sweden, low and medium level radioactive waste will be located in hard rock caverns, at a depth of 50 metres below the sea bottom. A typical geometry of a cavern is 6 metres width, 15 metres height and 150 metres length. In the area of Forsmark repository the sea water level is approximately 6 metres above the ground.

Chemical reactions in the stored waste will result in gas (hydrogen) production in a saturated water environment. Under such conditions the gas will displace the water from the fractures and migrate towards the surface and escape through the sea bottom.

The study on the conditions of gas migration from low level repositories was the subject of a previous report (SKBF-KBS: 83-21). This investigation presents a numerical model developed for the computation of gas-water displacement in hard rock formations. Calculations are presented for the Forsmark low level repository conditions.

The upper part of fractured rock formations is characterized by a relatively large fracture frequency and good fracture connectivity. Under such conditions, due to the large difference in density between hydrogen and water, the lateral gas-water displacement extent will be negligible and the flow will be essentially vertical.

The rock permeability was determined in vertical boreholes mainly by double packer tests. The high fracture permeability suggests that the radius of influence during the test was large enough to imply that the effect of the connectivity between the fractures is reflected in the measured permeability. The permeability distribution of these boreholes was considered to be representative also for the horizontal direction along the repository cavern. Only the results over the first 50 metres below the sea level were considered. The fracture frequency varies in general between 1 and 10 fractures per metre. Exceptionally, over very limited regions, fractures are not present at all.

Because of the lack of knowledge on the fracture network geometry and on the individual fracture details, solutions for real configurations of fractured rock formations are not possible. Instead, fictitious medium equivalents such as porous media, fracture planes or capillary tubes models may be considered for convenience.

In the present calculations the rock mass is conceptualized as a discontinuous system of fracture planes intersecting the rock cavern. This model approach is considered to represent better the actual flow phenomena associated with gas-water displacement in a fractured rock mass than the continuum approach.

The displacement process is characterized by a faster advance of the gas through the fractures of high permeability than those of low permeability. In a flow problem with a constant gas source in the cavern the breakthrough in the large fractures causes a drop in pressure at the cavern. As a result, there is no further advance of the gas through the small fractures and backflow will occur.

This means that the present flow problem is dominated by the fractures of high permeability. In individual fractures there is a sharp interface between the displacing and the displaced fluid. Therefore, the sharp interface approach was considered in the present study for treating the displacement process in the discrete fracture planes.

2. EQUATIONS OF FLOW

In an individual fracture the displacing and the displaced fluids are separated by a sharp interface. Then in each flow region, gas and water, the flow is governed by the single phase flow momentum (Darcy's law) and mass balance equations. These equations are coupled through the capillary pressure at the interface.

(i) Gas flow equations

Darcy's law is

$$u_j^g = -\frac{k^g}{\mu^g}(p^g{}_{,j} - \rho^g g_j) \tag{1}$$

the mass conservation equation is

$$(\phi^g \rho^g)_{,t} + (\rho^g u_i^g)_{,i} + Q^g = 0 \tag{2}$$

where u is specific flux, k is permeability, μ is dynamic viscosity, ϕ is porosity, p is pressure, g is the acceleration of gravity and Q^g is the mass rate of gas production. Upperscript g denotes the gas phase, ϕ^g and k^g are porosity and permeability at the irreducible water saturation.

Expanding the time derivative, one obtains

$$(\phi^g \rho^g)_{,t} = \phi^g \rho^g{}_{,t} + \rho^g \phi^g{}_{,t} \tag{3}$$

The density of the gas is related to pressure through the equation of state.

$$\rho^g = \frac{p^g M}{Z\bar{R}T} \tag{4}$$

where M is the molecular weight to the gas, R is the universal gas constant, T is temperature and Z is the deviation factor of a real gas from the ideal gas behaviour and is a function of pressure and temperature.

The compressibility of the rock matrix is defined as

$$c^r = \frac{1}{\phi^g} \frac{d\phi^g}{dp^g} \tag{5}$$

Substituting the relationships (4) and (5) into (3), we obtain

$$(\phi^g \rho^g)_{,t} = \frac{\phi^g M}{Z\bar{R}\bar{T}} (1 + p^g c^r)\, p^g_{,t} \tag{6}$$

In equation (6) the value of $p^g c^r << 1$ and the equation may therefore be approximated as

$$(\phi^g \rho^g)_{,t} = \frac{\phi^g M}{Z\bar{R}\bar{T}}\, p^g_{,t} \tag{7}$$

Substitution of equation (7) together with Darcy's law into equation (2), yields

$$\frac{\phi^g M}{Z\bar{R}\bar{T}}\, p^g_{,t} - \left(\frac{k^g}{\mu^g} \frac{p^g M}{Z\bar{R}\bar{T}} \left(p^g_{,i} - \frac{p^g M}{Z\bar{R}\bar{T}}\, g_i\right)\right)_{,i} + Q^g = 0 \tag{8}$$

or

$$\phi^g \rho^g_{,t} - \left(\frac{k^g}{\mu^g} \rho^g \left(p^g_{,i} - \frac{p^g M}{Z\bar{R}\bar{T}}\, g_i\right)\right)_{,i} + Q^g \frac{ZRT}{M} = 0 \tag{9}$$

Equation (9) is highly non-linear and must therefore be solved by an iterative numerical scheme.

(ii) Water flow equations

Darcy's law is

$$u_j^w = -\frac{k^w}{\mu^w}(p^w_{,j} - \rho^w g_j) \tag{10}$$

and the equation for the conservation of mass is

$$(\phi^w \rho^w)_{,t} + (\rho^w u_i^w)_{,i} = 0 \tag{11}$$

where superscript w denotes the water phase, ϕ^w and k^w are porosity and permeability at the residual gas saturation.

Expanding the time derivative in equation (11), one obtains

$$(\phi^w \rho^w)_{,t} = \phi^w \rho^w c^w p_{,t} + \phi^w \rho^w c^r p_{,t} = c\phi^w \rho^w p_{,t} \tag{12}$$

where $c = c^w + c^r$ is the total (water and rock) compressibility

Substitution of equation (12) and Darcy's law into equation (11) yields

$$\phi^w \rho^w c\, p_{,t} - (\frac{k^w}{\mu^w} \rho^w (p^w_{,i} - \rho^w g_i))_{,i} = 0 \tag{13}$$

(iii) Gas-water interface

Across the gas-water interface there is a jump in pressure with a value given by the capillary pressure p_c, i.e.

$$p_g = p_w + p_c \tag{14}$$

A point located at the interface, on the side of the water or the side of the gas should move with the same velocity, which may be expressed by

$$v^g = v^w \tag{15}$$

Solving the flow problem implies solving equations (9), (13), (14) and (15) together with the appropriate boundary and initial conditions.

3. METHOD OF SOLUTION

The flow equations are solved using the Galerkin finite element method. The moving gas-water front requires a time adaptive element mesh with the finest discretization in the front region.

Gas-water interface

Relating the velocities to Darcy's law in the equation for the condition at the gas-water interface, we obtain

$$-\frac{k^g}{\phi^g \mu^g}\left(p^g_{,j} - \rho^g g_j\right) = -\frac{k^w}{\phi^w \mu^w}\left(p^w_{,j} - \rho^w g_j\right) \tag{16}$$

Rearranging the previous equation, we obtain

$$\frac{k^w}{\phi^w \mu^w} p^w_{,j} - \frac{k^g}{\phi^g \mu^g} p^g_{,j} = \left(\frac{k^w w}{\phi^w \mu^w} - \frac{k^g g}{\phi^g \mu^g}\right) g_j \tag{17}$$

or

$$\alpha_2 p^w_{,j} - \alpha_1 p^g_{,j} = (\beta_2 - \beta_1)\, g_j \tag{18}$$

where

$$\alpha_1 = \frac{k^g}{\phi^g \mu^g}, \quad \alpha_2 = \frac{k^w}{\phi^g \mu^g}, \quad \beta_1 = \frac{g_k{}^g}{\phi^g \mu^g}, \quad \beta_2 = \frac{w_k{}^w}{\phi^w \mu^w}$$

The interface equations are approximated as

$$\frac{\alpha_1}{\Delta l_1} p^g - \left(\frac{\alpha_1}{\Delta l_1} + \frac{\alpha_2}{\Delta l_2}\right) p^i + \frac{\alpha_2}{\Delta l_2} p^w - (\beta_2 - \beta_1)\, g_j = 0 \tag{19}$$

where superscript i denotes an interface node and

$$\Delta l_1 = x^i - x^g, \quad \Delta l_2 = x^w - x^i$$

The algebraic equations for the interface nodes and those of the flow equations for the two phases are solved simultaneously.

Finite element formulation of the flow equations

The two flow equations for gas and water have the general form

$$\alpha p_{,t} - (\beta (p_{,i} - \rho g_i))_{,i} + Q = 0 \tag{20}$$

In the water phase α denotes $\phi\rho^w c$, β denotes $\rho^w k^w/\mu^w$ and ρ denotes ρ^w. In the gas phase α denotes ϕ^g , β denotes $p^g k^g/\mu^g$ and ρ denotes $p^g M/ZRT$.

Applying Galerkin's method, we obtain

$$\int_R \alpha p_{,t} \psi^I \, dR - \int_R (\beta(p_{,i} - \rho g_i))_{,i} \psi^I \, dR + \int_R Q \psi^I \, dR = 0 \tag{21}$$

where I is 1,2,...M-1 in the gas phase, I is M+1,M+2,...N in the water phase, M represents an interface node, N is the total number of nodes and ψ^I is the weighting function. Using Green's theorem, we obtain.

$$\int_R \alpha p_{,t} \psi^I dR + \int_R (\beta(p_{,i} - \rho g_i)) \psi^I_{,i} dR - \int_\Gamma q^n \psi^I \, dR + \int_R Q \psi^I dR = 0 \tag{22}$$

For simplicity we assume that the gas source is represented by the source term (Q) and that there are no additional boundary sources to be accounted for. Then the integral along the boundary vanishes. The time derivative term is approximated by the finite difference method. Then we may write the previous equation as

$$\int_R \alpha \frac{\Delta p}{\Delta t} \psi^I dR + \int_R \beta p_{,i} \psi^I_{,i} \, dR - \int_R \beta\rho g_j \psi^I_{,i} dR + \int_R Q \psi^I dR = 0 \tag{23}$$

Pressure and functional coefficients are approximated as

$$p = P^J \psi^J, \quad \alpha = \alpha^K \psi^K, \quad \beta = \beta^K \psi^K \tag{24}$$

Then equation (23) may be written as

$$\alpha^K \frac{\Delta p^J}{\Delta t} \int_R \psi^K \psi^J \psi^I \, dR + \beta^K p^J \int_R \psi^J_{,i} \, \psi^I_{,i} \, dR - \beta^K \rho^J g_j \int_R \psi^K \psi^J \psi^I_{,i} \, dR + \int_R Q \, \psi^I \, dR = 0 \qquad (25)$$

The integrals are solved numerically by Gauss integration. The flow equations represented by equation (25) are assembled together with the algebraic equations resulting from the interface equations (19). A fully implicit scheme is adopted and finally the matrix problem to be solved becomes

$$[A]\{p\} = \{B\} \qquad (26)$$

Equation (26) represents a non-symmetric system of sparse linear equations which is solved by Gauss elimination using the frontal method.

Numerical treatment of prescribed gas flux condition

The flow problem is simultaneously solved for each fracture category in an iterative way. For simplicity, it is assumed that the fractures can be divided into a small number of categories. The total gas flux from the cavern is obtained by adding the fluxes for each fracture category. The computed total flux is then compared with the known gas production and the pressure is adjusted iteratively using a Newton-Raphson technique until the stipulated accuracy is achieved.

The total flux (Q) is

$$Q = \sum_{i=1}^{k} n_i Q_i \tag{27}$$

where k is the number of fracture categories, n_i is the number of fractures in category i, and Q_i is the flux computed for fracture category i.

The flux condition may be expressed as

$$Q(p) = Q_o \tag{28}$$

where Q_o denotes the rate of the total gas production.

Expanding the left hand side in a Taylor series we obtain

$$Q(p_o) + (p - p_o) \left.\frac{dQ}{dp}\right|_{p=p_o} + (\text{higher order terms}) = Q_o \tag{29}$$

Neglecting the higher order terms, we obtain

$$Q(p_o) + (p - p_o) \frac{dQ}{dp} = Q_o \tag{30}$$

Rearranging equation (30) we obtain

$$p = p_o + \frac{dp}{dQ} (Q_o - Q(p_o)) \tag{31}$$

which is approximated as

$$p^{(i+1)} = p^{(i)} + \frac{p^{(i+1)} - p^{(i)}}{Q^{(i+1)} - Q^{(i)}} (Q_o - Q^{(i+1)}) \tag{32}$$

where i denotes the current iteration level.

RESULTS

The calculations performed gave evidence for a rather high transport capacity of the rock mass considered and the gas could readily escape through high permeability class of fractures in the fracture network considered. The initial hydrostatic pressure is exceeded only during a few minutes in the initial stage. It should be pointed out that the gas flux is imposed as an instanenous gas source in the calculations.

The calculations were carried out for a total gas production of 10^{-3} kg/s. This figure corresponds to a total gas production of 400000 Nm^3/year (about 33000 kg/year) and is considered to be the maximum possible gas production rate for the cavern considered (150x6x15 metres). Calculations were also carried out for a prescribed gas cushion of 0.5 metres.

In solving simultaneously for the assumed fracture distribution of 6 fracture classes given in Table 2 (for a derivation of these see Appendix) it could be observed that displacement occurred mainly in the fractures of the high permeability. After breakthrough at the sea bottom there was a sudden drop in pressure and subsequently no further displacement took place in the low permeability fractures. The pressure drop even caused backflow in the low permeability fracture classes. Generally, the transport capacity of the gas increases several orders of magnitudes after the breakthrough.

In consequence of the fact that the flow problem under the present conditions essentially is governed by the high permeability class of fractures we directed the analysis towards this fracture class. Calculations were carried out assuming that the rock cavern was intersected by 18 ideal fracture planes with a permeability of $1.8*10^{-8} m^2$ ($b=4.65*10^{-4}$ m). The results of these calculations are presented in Figures 1, 2 and 3. The difference between the initial pressure buildup in the cavern for all six fracture classes and the high permeability class was only about 0.15 bars, which substantiates the fact the present flow problem is governed by the high permeability fractures.

Prescribed gas flux

Figure 1 shows the pressure distribution and the position of the gas-water interface at various points of time for a constant gas source of 10^{-3} kg/sec. As can be observed in the figure there is an instantaneous pressure build-up immediately after the gas source has been applied. However, only after about 5 minutes the pressure drops until the initial hydrostatic pressure, which is about 6.5 bars. The breakthrough time to the sea bottom is about 15 minutes. After breakthrough, the pressure drops suddenly and steady state conditions are reached almost instantaneously.

Figure 2 shows the gas-water displacement as a function of time and Figure 3 shows the pressure at the cavern roof as a function of time. As one can see the displacement velocity increases with time. Subsequently, the pressure drop increases with time until the breakthrough at the sea bottom. The maximum initial pressure required to initiate displacement (corresponding to the lowest permeability fracture classs) is equivalent to a gas cushion of 0.5 metres ($0.5*10^{-4}$Pa) was considered relatively low and therefore neglected in the calculations.

Prescribed gas cushion

It is of interest to study the rate of gas flow when the flow problem is governed by the necessary pressure to initialize displacement. As the maximum gas cushion required to initiate displacement is 0.5 metres for the low permeability fracture class, this value was used in the calculations.

Figure 4 shows the pressure distribution and the position of the gas-water interface at various points of time for an assumed constant gas cushion at the cavern top of 0.5 metres. As can be observed the gas displaces the water very fast and the breakthrough at the sea bottom occurs after about 40 minutes. As in the previous setting there is a sudden drop in pressure after the breakthrough at the sea bottom and steady state conditions are reached almost instantaneously.

Figure 5 shows the gas-water displacement as a function of time and Figure 6 shows the total mass rate of the gas at cavern roof as a function of time. Figure 5 looks very much the same as Figure 2 (with constant gas flux conditions at cavern top). Figure 6 represents less realistic conditions from the point of view that keeping constant pressure at the cavern top constant requires that the rate of the gas production increases continuosly with time.

It is however of significant interest in the present circumstances to know the order of the magnitude of the gas rate. The results of the calculations, graphically displayed in Figure 6, show that the total gas rate after breakthrough is about 0.4 kg/sec, which is about 350 times larger than the constant gas rate assumed in the previous setting, i.e. 33000 kg/year considered to be the largest possible rate of gas production.

The values of the input parameters used in the calculations are presented in Table 1 and the fracture distribution data are given in Table 2.

Table 1: Input parameter values

Parameter	Symbol	Value	Units
compressibility of water	c^w	10^{-10}	Pa^{-1}
rock compressibility	c^r	0.0	Pa^{-1}
density of water	ρ^w	999	kgm^{-3}
dynamic viscosity of water	μ^w	$1.307*10^{-3}$	^{r}as
density of the gas	ρ^g	$g = \frac{p^g M}{Z\bar{R}T}$	kgm^{-3}
dynamic viscosity of the gas	μ^g	$8.5*10^{-6}$	Pas
molecular weight of hydrogen	M	2.016	kg $mole^{-1}$
universal gas constant	R	8.3143	J $mol^{-1}K^{-1}$
temperature	T	283.16	K
devation factor for real gases	Z	Z = Z(p,T,M,R)	-

Table 2: Fracture distribution data

Class	Fracture width	Frequency
1	$3.986*10^{-5}$	18
2	$4.305*10^{-5}$	18
3	$6.319*10^{-4}$	99
4	$1.082*10^{-4}$	90
5	$1.648*10^{-4}$	45
6	$4.648*10^{-4}$	18

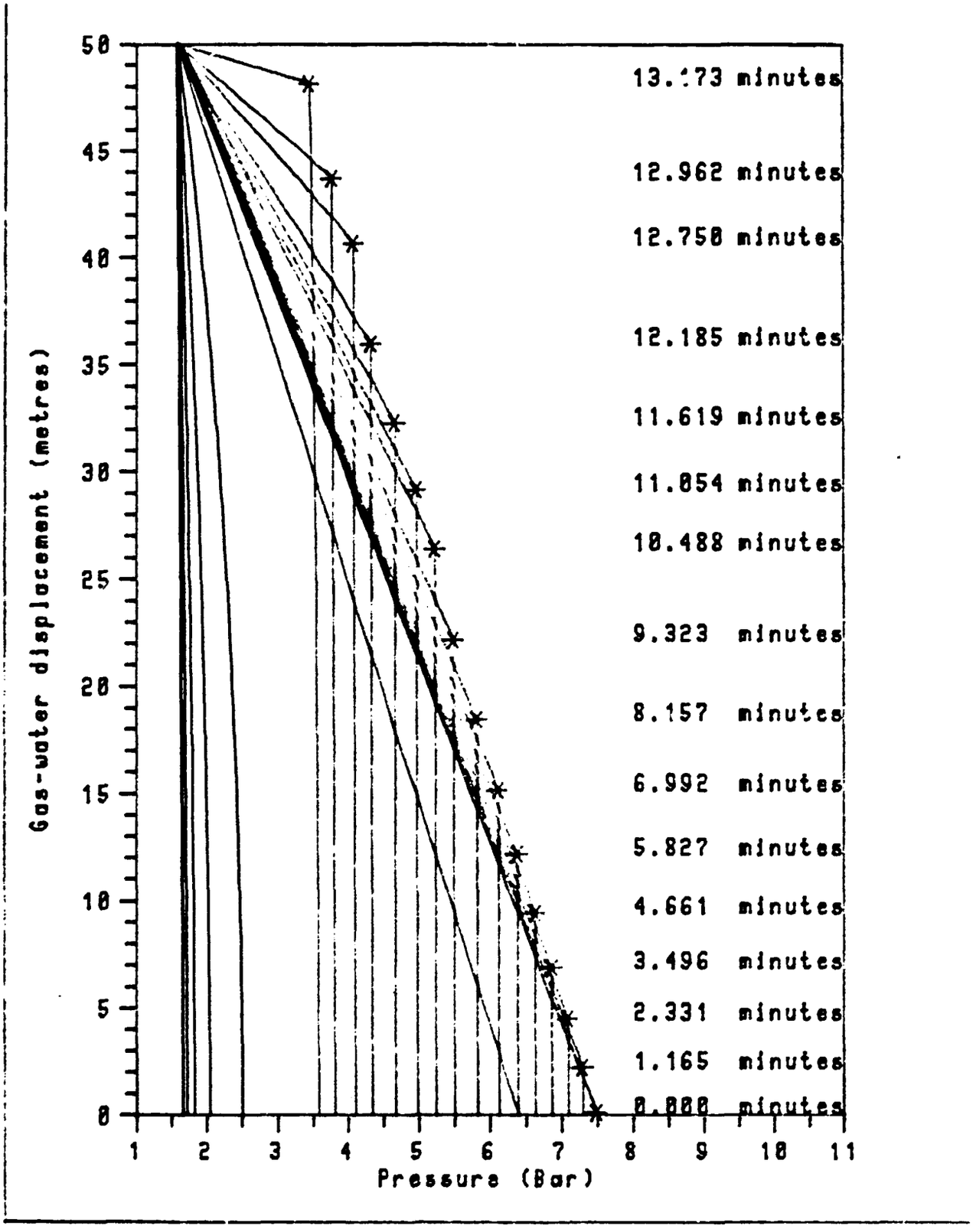

Figure 1. Gas-water displacement display for the class of fractures with a fracture permeability of $1.8*10^{-8}m^2$. The gas production is 10^{-3}kg/sec. The solid lines show the pressure distribution for various positions of the interface and the asterisks denote the position of the gas-water interface at various points of time.

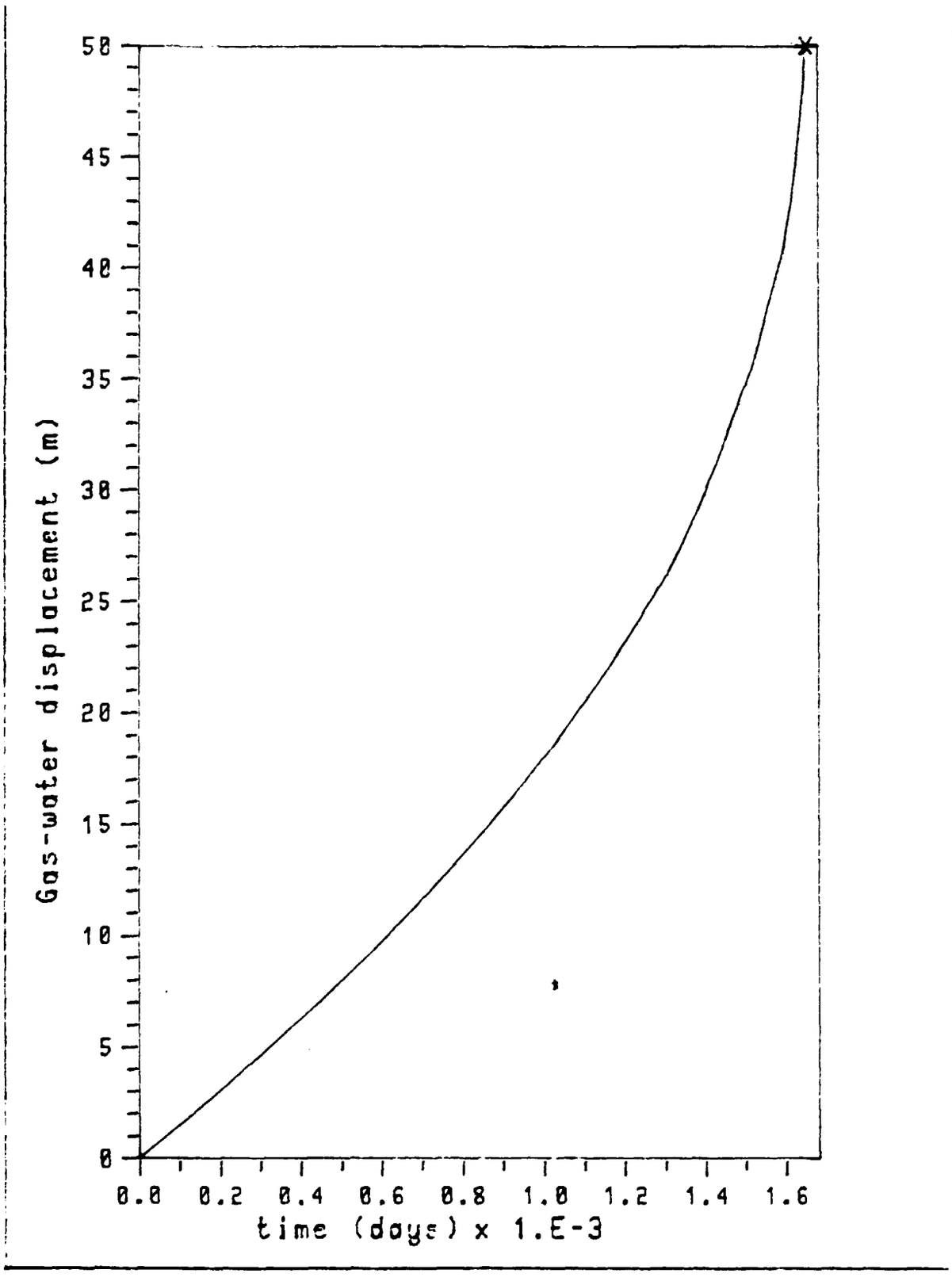

Figure 2. Location of the interface as a function of time for the class of fractures with a fracture permeability of $1.8*10^{-8}$ m^2. The gas production is 10^{-3}kg/sec. The asterisk denotes the breakthrough time.

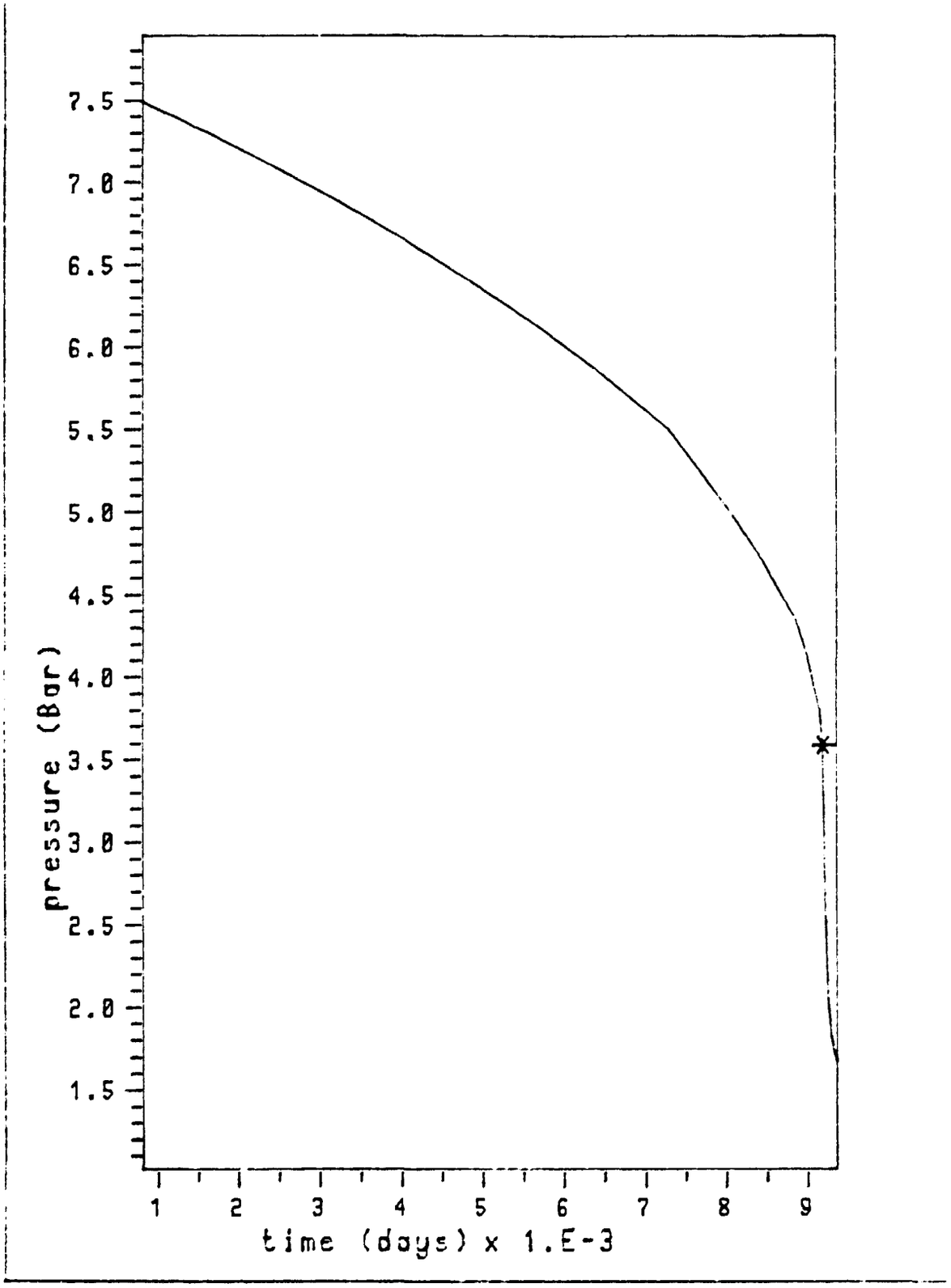

Figure 3. Pressure at cavern top as a function of time for the class of fractures with a fracture permeability of $1.8*10^{-8}$ m^2. The gas production is 10^{-3}kg/sec. The asterisk denotes the breakthrough time.

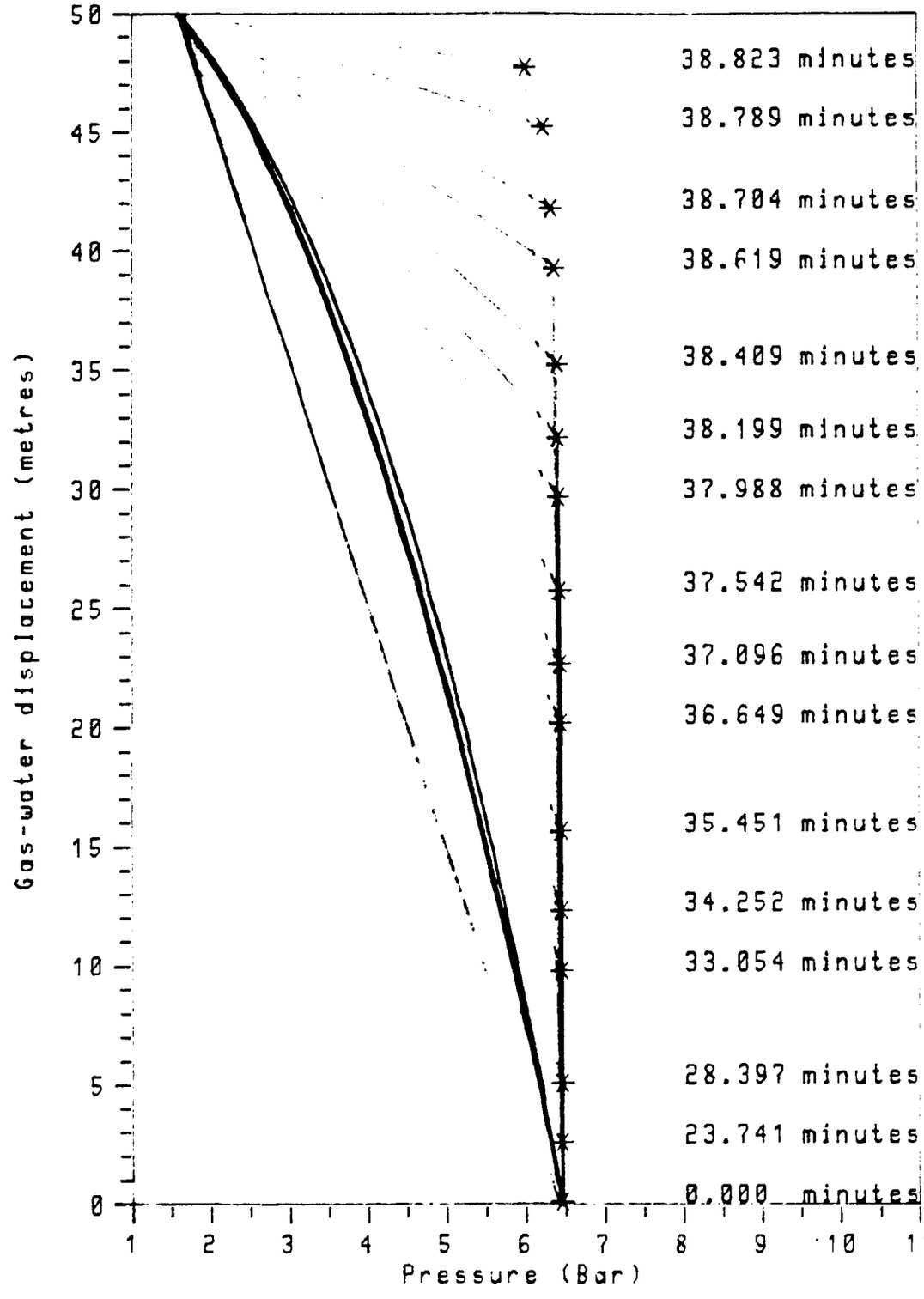

Figure 4. Gas-water displacement display for the class of fractures with a fracture permeability of $1.8*10^{-8}$ m^2 and a gas cushion of 0.5 metres. The solid lines show the pressure distribution for various positions of the interface and the asterisks denote the position of the gas-water interface at various points of time.

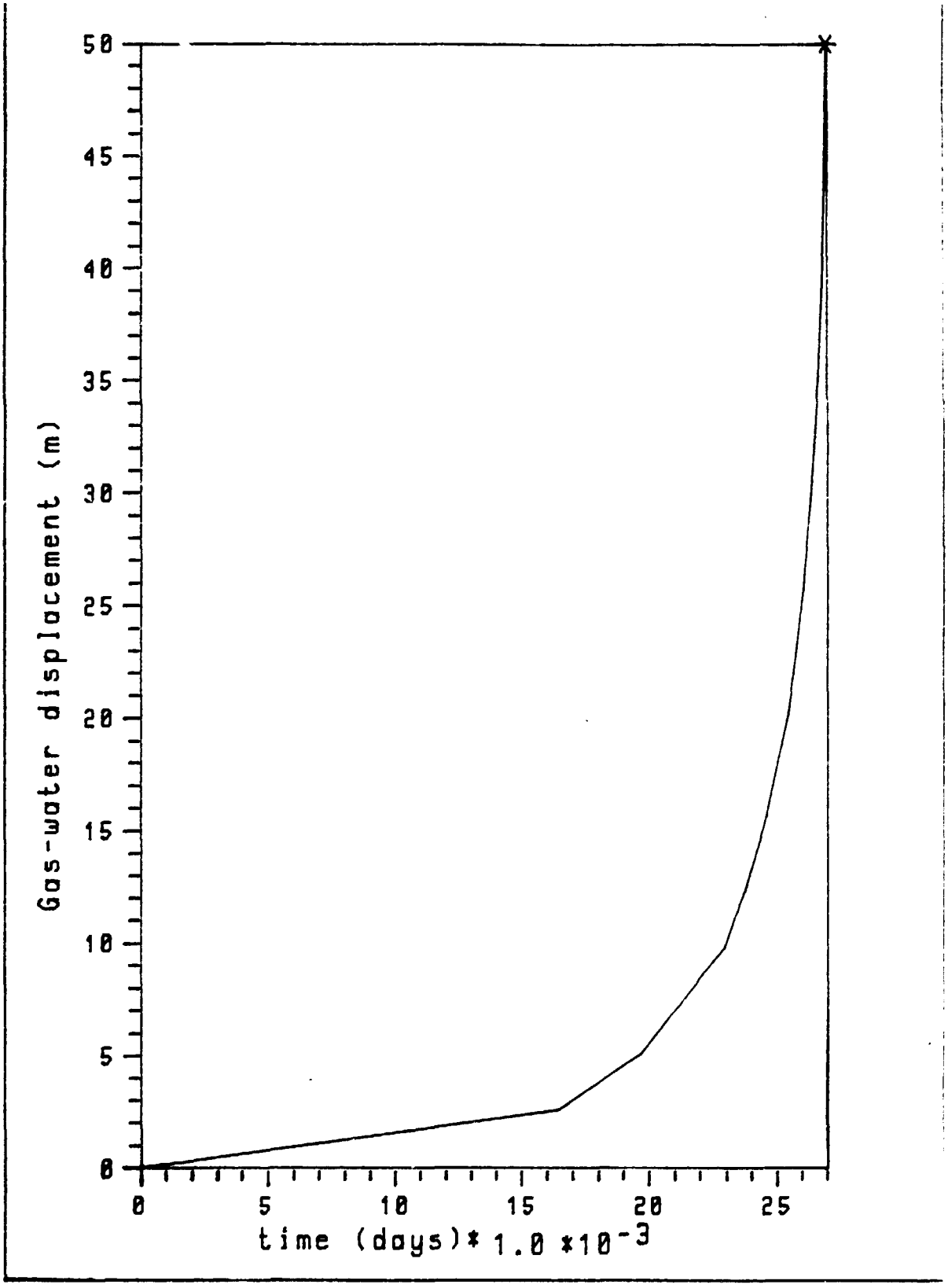

Figure 5. Location of the interface as a function of time for the class of fractures with a fracture permeability of $1.8*10^{-8}$ m^2 and a gas cushion of 0.5 metres. The asterisk denotes the breakthrough time.

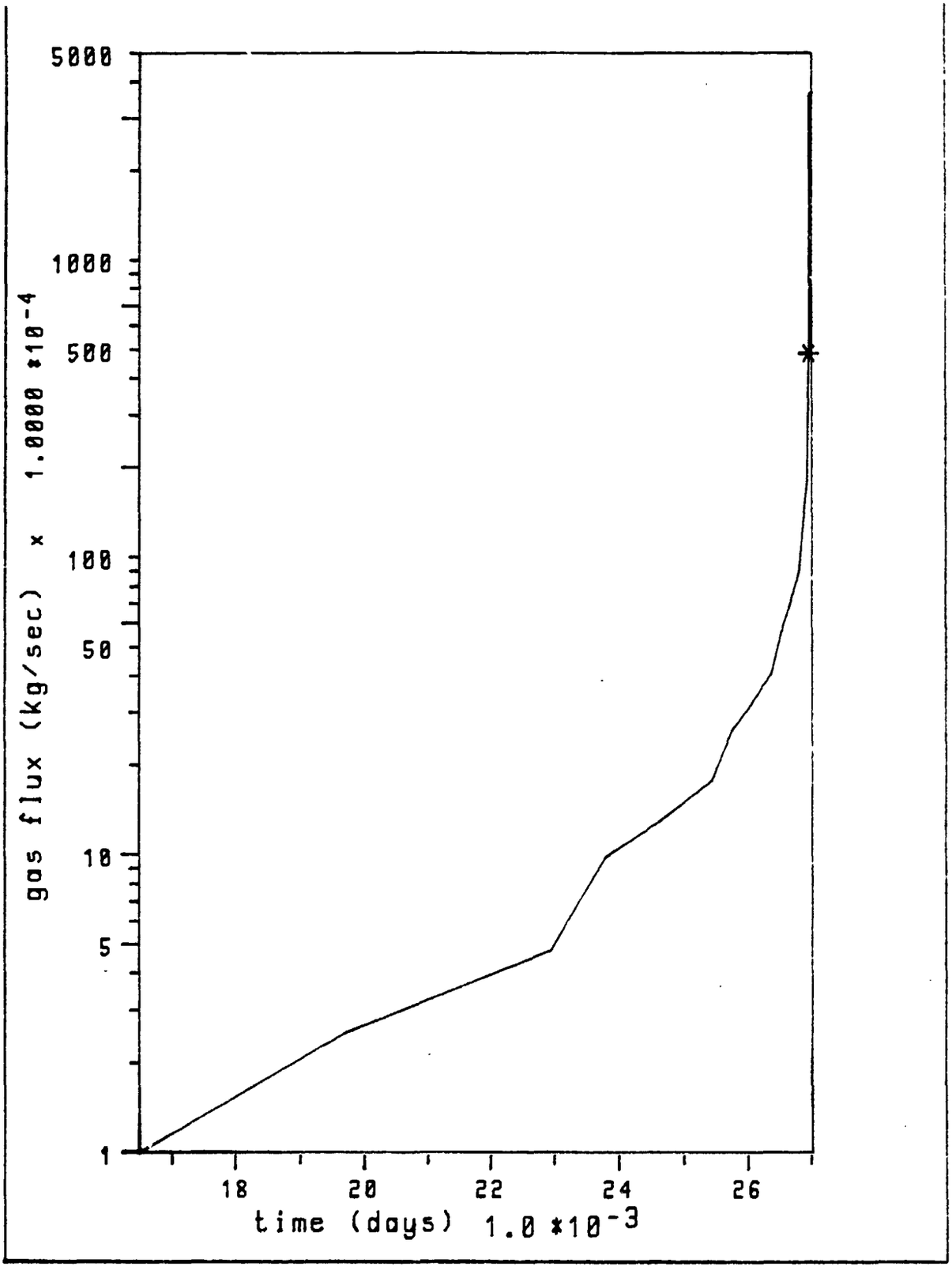

Figure 6. Total gas flow rate as a function of time for the class of fractures with a fracture permeability of $1.8*10^{-8}$ m^2 and a gas cusion of 0.5 metres. The asterisk denotes breakthrough time.

REFERENCES

1. Braester, C., Thunvik, R., 1983, An analysis of the conditions of gas migration from a low-level radioactive waste repository, SKBF-KBS: 83-21.

2. Carlsson, L., Carlsten, S., Sigurdsson, T., Winberg, A., 1985, Hydraulic Modeling of The Final Repository for Reactor Waste (SFR), Swedish Geological Co., - Compilation and Conceptualization of Available Geological and Hydrological Data, Swedish Geological Co. IRAP 85406.

ACKNOWLEDGMENT

The first author is sponsored by the Swedish Natural Science Council.

Appendix A: CALCULATION OF ROCK PROPERTIES IN THE FORSMARK AREA

Rock permeability

Rock permeabilitites in the Forsmark area were presented by Carlsson et al. (1985). In most cases permeabilities were determined by double packer tests within an interval of three metres. Permeability values of the first metres below the surface are seldom available. Table A1 gives the available values for the first 50 metres below the ground surface.

Table A1: Hydraulic conductivities (log K) along the boreholes

Borehole KB-1

length (m)	log(K) (K-m/s)
3.0	-7.7
3.0	-6.8
3.0	-7.7
3.0	-7.7
3.0	-7.7
3.0	-5.6
3.0	-7.0
3.0	-7.7
3.0	-7.7
3.0	-7.7
3.0	-7.3
3.0	-7.9

Table A1: Continued

Borehole KB-2

length (m)	log(K) (K-m/s)
3.0	-7.5
3.0	-7.7
3.0	-7.7
3.0	-7.1
3.0	-7.3
3.0	-7.7
3.0	-7.2
3.0	-6.8
3.0	-6.5
3.0	-7.5
3.0	-6.7
3.0	-7.7

Borehole KB-3

length (m)	log(K) (K-m/s)
3.0	-5.7
3.0	-6.8
3.0	-4.9
3.0	-6.7
3.0	-7.7
3.0	-5.4
3.0	-5.3
3.0	-6.5
3.0	-6.5

Table A1: Continued

Borehole KB-4

length (m)	log(K) (K-m/s)
3.0	-6.0
3.0	-6.4
3.0	-7.2
3.0	-7.0
3.0	-6.5
3.0	-6.6
3.0	-7.7
3.0	-7.7
3.0	-6.6
3.0	-6.5
3.0	-6.4
3.0	-6.4

Borehole KB-5

length (m)	log(K) (K-m/s)
3.0	-6.3
3.0	-6.2
3.0	-6.3
3.0	-6.5
3.0	-6.6
3.0	-6.3
3.0	-6.6
3.0	-6.4
3.0	-6.0
3.0	-6.2
3.0	-6.0
3.0	-6.1

Table A1: Continued

Borehole KB-11

length (m)	log(K) (K-m/s)
3.0	-7.7
3.0	-7.7
3.0	-7.7
3.0	-7.7
3.0	-7.7
3.0	-7.7
3.0	-7.7
3.0	-7.7

Borehole KB-12

length (m)	log(K) (K-m/s)
3.0	-7.5
3.0	-7.7
3.0	-7.7
3.0	-7.7
3.0	-7.7
3.0	-7.7
3.0	-7.7
3.0	-7.7

Table A1: Continued

Borehole KB-13

length (m)	log(K) (K-m/s)
3.0	-7.7
3.0	-7.7
3.0	-7.7
3.0	-7.7
3.0	-7.7
3.0	-7.7
3.0	-7.7

Borehole KB-14

length (m)	log(K) (K-m/s)
3.0	-7.1
3.0	-6.9
3.0	-7.7
3.0	-7.7
3.0	-7.7
3.0	-7.5
3.0	-7.7
3.0	-7.7

Table A1: Continued

Borehole KB-15

length (m)	log(K) (K-m/s)
3.0	-7.7
3.0	-6.3
3.0	-7.7
3.0	-7.7
3.0	-7.7
3.0	-7.7

Borehole KB-16

length (m)	log(K) (K-m/s)
3.0	-5.7
3.0	-7.7
3.0	-7.7
3.0	-6.3
3.0	-6.4
3.0	-7.8
3.0	-7.2
3.0	-6.1

Table A1: Continued

Borehole KB-17

length (m)	log(K) (K-m/s)
3.0	-6.8
3.0	-7.2
3.0	-7.1
3.0	-6.2
3.0	-6.7
3.0	-7.6
3.0	-7.2
3.0	-7.3
3.0	-7.2

Borehole KB-18

length (m)	log(K) (K-m/s)
3.0	-7.0
3.0	-6.7
3.0	-5.8
3.0	-6.7
3.0	-6.7
3.0	-5.7
3.0	-7.8
3.0	-6.4
3.0	-7.8

Table A1: Continued

Borehole DS-9

length (m)	log(K) (K-m/s)
3.0	-7.7
3.0	-7.7
3.0	-7.7
3.0	-7.7
3.0	-7.3
3.0	-7.7
3.0	-7.7
3.0	-7.7
3.0	-7.7

Borehole DS-10

length (m)	log(K) (K-m/s)
3.0	-3.6
3.0	-3.7
3.0	-6.7
3.0	-7.0
3.0	-7.7
3.0	-7.7
3.0	-6.2
3.0	-6.1
3.0	-5.8
3.0	-6.5
3.0	-7.8
3.0	-7.8
3.0	-5.3
3.0	-7.8
3.0	-6.5

Permeability frequency

Permeability and the number of appearences are calculated and given Table A2 using the data from Table A1.

Table A2: Permeability and number of observations (over sections of 3 metres)

Class	permeability	nr. of observations
1	0.12589E-13	1
2	0.15849E-13	6
3	0.19953E-13	58
4	0.25119E-13	1
5	0.31623E-13	4
6	0.50119E-13	4
7	0.63096E-13	6
8	0.79433E-13	3
9	0.10000E-12	4
10	0.12589E-12	1
11	0.15849E-12	4
12	0.19953E-12	7
13	0.25119E-12	4
14	0.31623E-12	8
15	0.39811E-12	6
16	0.50119E-12	5
17	0.63096E-12	4
18	0.79433E-12	3
19	0.10000E-11	3
20	0.15849E-11	2
21	0.19953E-11	3
22	0.25119E-11	1
23	0.39811E-11	1
24	0.50119E-11	2
25	0.12589E-10	1
26	0.19953E-09	1
27	0.25119E-09	1

Total number of observations: 144

We shall assume that the probability distribution function for the rock inhomogeneities is isotropic and homogeneous. Under this assumption samples along the vertical boreholes are representative also for the horizontal section along the repository.

The total number of 144 observations extends over a length of 432 metres. For the considered length of the cavern of 150 meters the number of observations are reduced proportionally. For the sake of convenience we have lumped several classes into the same class, resulting in six distribution classes. The number of appearences over the corresponding cavern length and the average permeability for each class are presented in Table A3.

The fracture frequency varies between zero and 10 fractures per metre. It seems that the most frequent is 3 fractures per metre. This figure will be considered in the following calculations. There is no correlation between fracture frequency and permeability.

Calculation of fracture permeability and rock porosity

Fracture permeability and porosity are calculated indirectly considering an ideal fracture plane model. Fracture permeability is then

$$k^f = \frac{b^2}{12} \qquad (A1)$$

and the relationship between fracture permeability and rock permeability is expressed as

$$k^f bB = K1B \qquad (A2)$$

where b is the fracture width, B is the cavern width, k is the rock permeability and l is the fracture spacing. Substituting equation (A1) into (A2) and solving for b, we obtain

$$b = (12kl)^{1/3} \qquad (A3)$$

The formation porosity is

$$\phi = b/l \tag{A4}$$

or

$$\phi = \left(\frac{12k}{l^2}\right)^{1/3} \tag{A5}$$

The calculated fracture permeabilities using equation (A3) and porosities using equation (A5) are given in Table A3.

Table A3: Parameter values for the six distribution classes

class	length along cavern (m)	nr.of observ. over 150 m cavern*)	formation properties: permeability (sq.m)	formation properties: porosity (%)	equivalent properties for fract. plane model: fracture width (m)	equivalent properties for fract. plane model: number of fractures
1	6	2	0.1585E-13	1.1962E-04	3.9875-05	18
2	60	20	0.1995E-13	1.2916E-04	4.3053-05	18
3	33	11	0.6309E-13	1.8958E-04	6.3194-04	99
4	30	10	0.3162E-12	3.2444E-04	1.0815-04	90
5	15	5	0.1119E-11	4.9441E-04	1.6480-04	45
6	6	2	0.2511E-10	1.3945E-03	4.6484-04	18

*) refers to permeability average value measured over a length of 3 m.

Appendix B: ANALYTICAL VALIDATION OF THE MATHEMATICAL MODEL

An analytical solution may be obtained for a simplified model of one-dimensional flow, assuming that water and gas are incompressible. Owing to the strong dependence of the gas properties on pressure, the obtained solution may be used for problems in which the variation in pressure is relatively small, using average pressure dependent properties. In the present study the obtained analytical solution will be used for the validation of the numerical solution.

We consider the flow through a fracture plane of constant width (b). The fluids are assumed to be separated by a sharp interface. For one-dimensional flow in the s-direction, whose angle with the horizontal direction is α, the equations of flow are

In the gas region

Poiseuille law is

$$v_g = - \frac{k_f}{\mu_g} \frac{\partial \Phi_g}{\partial s} \qquad (B1)$$

where $\Phi_g = p_g + \rho_g g z$ and k_f is fracture permeability equal to $b^2/12$.

The equation of conservation of mass is

$$\frac{\partial v_g}{\partial s} = 0 \qquad (B2)$$

Substitution of eq. (B1) into (B2) yields

$$\frac{\partial^2 \Phi_g}{\partial s^2} = 0 \qquad (B3)$$

In the water region

Poiseuille law is

$$v_w = - \frac{k_f}{\mu_w} \frac{\partial \phi_w}{\partial s} \tag{B4}$$

where $\phi_w = p_w + \rho_w g z$

and the equation of conservation of mass is

$$\frac{\partial v_w}{\partial s} = 0 \tag{B5}$$

Substitution of eq. (B4) into (B5) yields

$$\frac{\partial^2 \phi_w}{\partial s^2} = 0 \tag{B6}$$

The considered boundary conditions are constant gas pressure at $s = 0$ and constant water pressure at $s = L$, where L is the fracture length, i.e.,

$$s = 0 \qquad \phi_g = \phi_{go} \tag{B7}$$

$$s = L \qquad \phi_w = \phi_{wL} \tag{B8}$$

At the water-gas interface $s = \xi$, the water and the front moves with the same velocities. From equations (B2) and (B5) it follows that in each phase and at each instant the velocities are constant. This result combined with the condition of constant velocities across the front, leads to the conclusion that at each instant the velocity is constant along the whole flow domain.

A second imposed condition is the constant capillary pressure (p_c) across the water-gas interface, i.e.

$$s = \xi \qquad p_c = p_{gz} - p_{wz} = \text{const.} \tag{B9}$$

Initially the fracture is assumed to be fully saturated by water, i.e.,

$$t = 0 \qquad \xi = 0 \tag{B10}$$

Integration of equations (B3) and (B6) with the prescribed boundary conditions expressed by eqs. (B7) and (B8) yields

$$\phi_g = \phi_{go} + \frac{\phi_{g\xi} - \phi_{go}}{\xi} s \tag{B11}$$

$$\phi_w = \phi_{w\xi} + \frac{\phi_{wL} - \phi_{w\xi}}{L - \xi} (s - \xi) \tag{B12}$$

which express the linear distribution of the potential ϕ, along the flow domain s.

Substitution of equations (B1) into (B11) yields

$$v_g = - \frac{k_f}{\mu_g} \frac{\phi_{go} - \phi_{g\xi}}{\xi} = \frac{k_f}{\mu_g} \frac{p_{go} - p_g - \rho_g g \xi \sin\alpha}{\xi} \tag{B13}$$

and substitution of equations (B5) into (B13) yields

$$v_w = - \frac{k_f}{\mu_w} \frac{\phi_w - \phi_{wL}}{L - \xi} = \frac{k_f}{\mu_w} \frac{p_{w\xi} - p_{wL} - \rho_w g (L-\xi) \sin\alpha}{L - \xi} \tag{B14}$$

Adding equations (B13) and (B14) and in which, as previously shown, v_g and v_w are equal, we obtain after some mathematical manipulations

$$v_g = -\frac{k_f}{\mu_g} \frac{p_{go} - p_{wL} - p_c - g\rho_w L\sin\alpha + g\Delta\rho\xi\sin\alpha}{\xi + \frac{\mu_w}{\mu_g}(L-\xi)} \tag{B15}$$

Equation (B15) gives the velocity of the gas as a function of the length of displacement ξ.

The advance of the water-gas front in time may be obtained by integrating the relationship between the advance of the front and the velocity

$$v_g = \frac{d\xi}{dt} \tag{B16}$$

in which v_g is expressed by eq. (B16), and obtain

$$t = \frac{\mu_g}{k_f} \frac{1}{g\Delta\rho\sin\alpha} \left[\left(\frac{\mu_w}{\mu_g} L - \frac{(1 - \frac{\mu_w}{\mu_g})(\Delta p - \rho_w g L\sin\alpha)}{g\,\Delta\rho\sin\alpha}\right) \cdot \right.$$

$$\left. \ln\left(1 + \frac{g\Delta\rho\xi\sin\alpha}{\Delta p - \rho_w g L\sin\alpha}\right) + \left(1 - \frac{\mu_g}{\mu_w}\right)\xi\right] \tag{B17}$$

where $p = p_{go} - p_{wL} - p_c$. Eq. (B17) holds for angles α different from zero.

The breakthrough time (t_b) of the gas at the exit face z = L is obtained by substituting $\xi = L$ in eq. (B17). Denoting by H the distance between the inflow and outflow faces along the vertical ($L = H/\sin\alpha$) we obtain

$$t_b = \frac{\mu_g}{k_f} \frac{1}{g\Delta\rho \sin^2\alpha} \left(\frac{\mu_w}{\mu_g} H - \frac{(1 - \frac{\mu_w}{\mu_g})(\Delta p - \rho_w g H)}{g\Delta\rho} \right) \cdot$$

$$\ln\left(1 + \frac{g\Delta\rho H}{\Delta p - \rho_w g H}\right) + \left(1 - \frac{\mu_g}{\mu_w}\right) H \qquad \text{(B18)}$$

The test case used for validation of the numerical model is presented in Figure B.1.

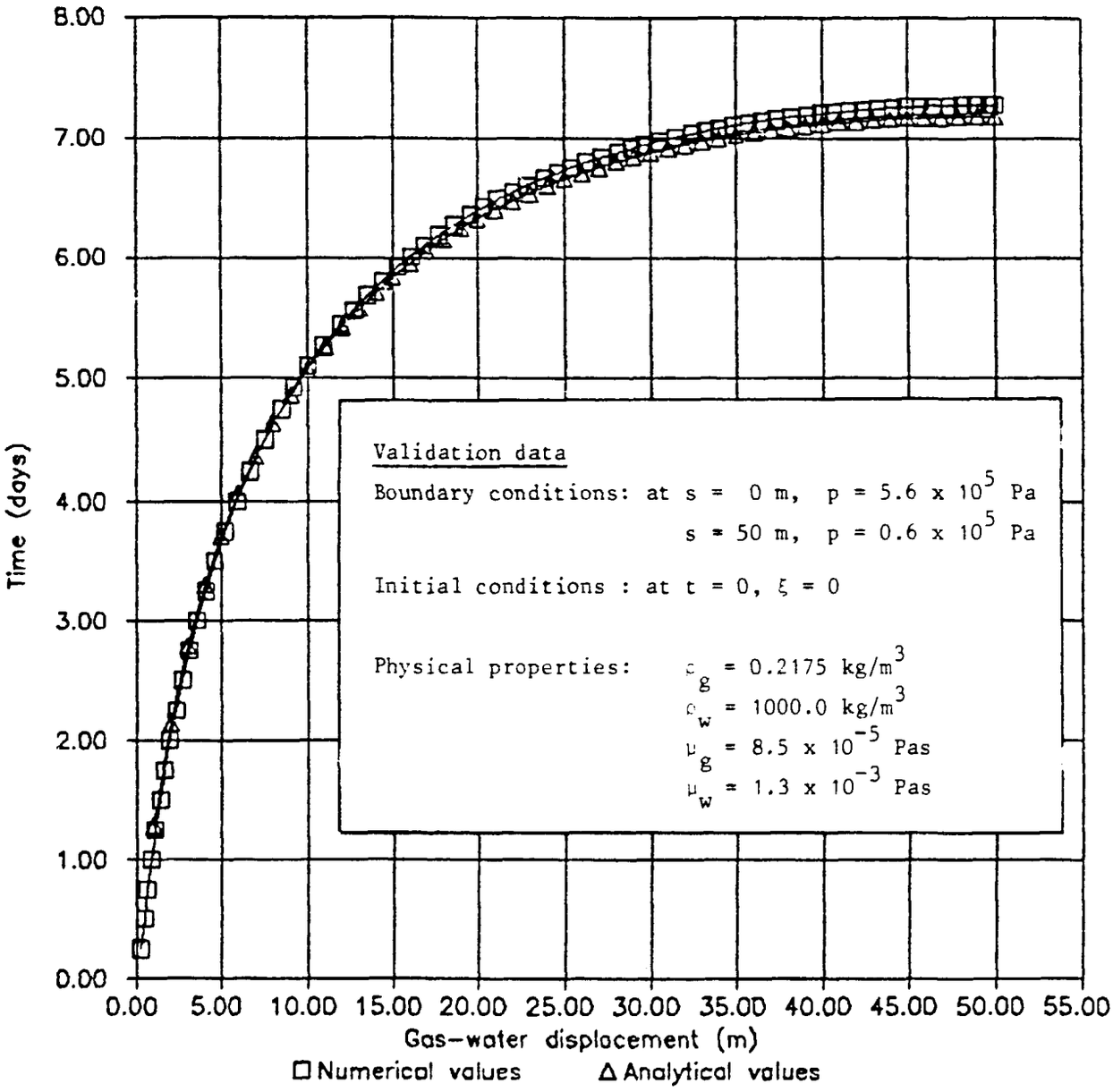

Figure B.1 Gas - Water displacement - test problem for validation of the numerical model

List of SKB reports

Annual Reports

1977–78
TR 121
KBS Technical Reports 1 – 120.
Summaries. Stockholm, May 1979.

1979
TR 79–28
The KBS Annual Report 1979.
KBS Technical Reports 79-01 – 79-27.
Summaries. Stockholm, March 1980.

1980
TR 80–26
The KBS Annual Report 1980.
KBS Technical Reports 80-01 – 80-25.
Summaries. Stockholm, March 1981.

1981
TR 81–17
The KBS Annual Report 1981.
KBS Technical Reports 81-01 – 81-16.
Summaries. Stockholm, April 1982.

1982
TR 82–28
The KBS Annual Report 1982.
KBS Technical Reports 82-01 – 82-27.
Summaries. Stockholm, July 1983.

1983
TR 83–77
The KBS Annual Report 1983.
KBS Technical Reports 83-01 – 83-76
Summaries. Stockholm, June 1984.

1984
TR 85–01
Annual Research and Development Report 1984
Including Summaries of Technical Reports Issued during 1984. (Technical Reports 84-01– 84-19)
Stockholm June 1985.

1985
TR 85-20
Annual Research and Development Report 1985
Including Summaries of Technical Reports Issued during 1985. (Technical Reports 85-01-85-19)
Stockholm May 1986.

1986
TR86-31
SKB Annual Report 1986
Including Summaries of Technical Reports Issued during 1986
Stockholm, May 1987

Technical Reports

1987
TR 87-01
Radar measurements performed at the Klipperås study site
Seje Carlsten, Olle Olsson, Stefan Sehlstedt, Leif Stenberg
Swedish Geological Co, Uppsala/Luleå
February 1987

TR 87-02
Fuel rod D07/B15 from Ringhals 2 PWR: Source material for corrosion/leach tests in groundwater
Fuel rod/pellet characterization program part one
Roy Forsyth, Editor
Studsvik Energiteknik AB, Nyköping
March 1987

TR 87-03
Calculations on HYDROCOIN level 1 using the GWHRT flow model
Case 1 Transient flow of water from a borehole penetrating a confined aquifer
Case 3 Saturated-unsaturated flow through a layered sequence of sedimentary rocks
Case 4 Transient thermal convection in a saturated medium
Roger Thunvik, Royal Institute of Technology, Stockholm
March 1987

TR 87-04
Calculations on HYDROCOIN level 2, case 1 using the GWHRT flow model
Thermal convection and conduction around a field heat transfer experiment
Roger Thunvik
Royal Institute of Technology, Stockholm
March 1987

TR 87-05
Applications of stochastic models to solute transport in fractured rocks
Lynn W Gelhar
Massachusetts Institute of Technology
January 1987

TR 87-06
Some properties of a channeling model of fracture flow
Y W Tsang, C F Tsang, I Neretnieks
Royal Institute of Technology, Stockholm
December 1986

TR 87-07
Deep groundwater chemistry
Peter Wikberg, Karin Axelsen, Folke Fredlund
Royal Institute of Technology, Stockholm
June 1987

TR 87-08
An approach for evaluating the general and localized corrosion of carbon steel containers for nuclear waste disposal
GP March, KJ Taylor, SM Sharland, PW Tasker
Harwell Laboratory, Oxfordshire
June 1987

TR 87-09
Piping and erosion phenomena in soft clay gels
Roland Pusch, Mikael Erlström,
Lennart Börgesson
Swedish Geological Co, Lund
May 1987

TR 87-10
Outline of models of water and gas flow through smectite clay buffers
Roland Pusch, Harald Hökmark,
Lennart Börgesson
Swedish Geological Co, Lund
June 1987

TR 87-11
Modelling of crustal rock mechanics for radioactive waste storage in Fennoscandia—Problem definition
Ove Stephansson
University of Luleå
May 1987

TR 87-12
Study of groundwater colloids and their ability to transport radionuclides
Kåre Tjus* and Peter Wikberg**
*Institute for Surface Chemistry, Stockholm
**Royal Institute of Technology, Inorganic Chemistry Stockholm
March 1987

TR 87-13
Shallow reflection seismic investigation of fracture zones in the Finnsjö area method evaluation
Trine Dahl-Jensen
Jonas Lindgren
University of Uppsala, Department of Geophysics
June 1987

TR 87-14
Combined interpretation of geophysical, geological, hydrological and radar investigations in the boreholes ST1 and ST2 at the Saltsjötunnel
Jan-Erik Andersson
Per Andersson
Seje Carlsten
Lars Falk
Olle Olsson
Allan Stråhle
Swedish Geological Co, Uppsala
1987-06-30

TR 87-15
Geochemical interpretation of groundwaters from Finnsjön, Sweden
Ignasi Puigdomènech[1]
Kirk Nordstrom[2]
[1]Royal Institute of Technology, Stockholm
[2]U S Geological Survey, Menlo Park, California
August 23, 1987

TR 87-16
Corrosion tests on spent PWR fuel in synthetic groundwater
R S Forsyth[1] and L O Werme[2]
[1]Studsvik Energiteknik AB, Nyköping, Sweden
[2]The Swedish Nuclear Fuel and Waste Management Co (SKB), Stockholm, Sweden
Stockholm, September 1987

TR 87-17
The July – September 1986 Skövde aftershock sequence
Conny Holmqvist
Rutger Wahlström
Seismological Department, Uppsala University
August 1987